Lowest Threshold Solar-Pumped Ce:Nd:YAG Laser with 2.06% Solar-to-TEM00 Mode Laser Conversion Efficiency

Dawei Liang, Joana Almeida, Miguel Catela, Hugo Costa, Dário Garcia, Bruno D. Tibúrcio, Emmanuel Guillot, Cláudia R. Vistas

Solar Energy Materials & Solar Cells 270 (2024) 112817

Contents lists available at ScienceDirect

Solar Energy Materials and Solar Cells

journal homepage: www.elsevier.com/locate/solmat

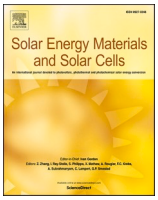

Lowest threshold solar-pumped Ce:Nd:YAG laser with 2.06% solar-to-TEM_{00} mode laser conversion efficiency

Dawei Liang [a,*], Joana Almeida [a], Miguel Catela [a], Hugo Costa [a], Dário Garcia [a], Bruno D. Tibúrcio [a], Emmanuel Guillot [b], Cláudia R. Vistas [a]

[a] Universidade NOVA de Lisboa, CEFITEC, Departamento de Física, FCT, 2829-516, Caparica, Portugal
[b] PROMES-CNRS, 66120, Font-Romeu-Odeillo-Via, France

ARTICLE INFO

Keywords:
Low-threshold
Ce:Nd:YAG
Fresnel lens
Solar laser
End-side-pumping

ABSTRACT

A solar-pumped laser with bulk active medium generally requires a considerable amount of concentrated solar power for initiating laser emission. In previous work, 54.9 W threshold incoming solar power was found for a Ce:Nd:YAG solar laser by a 0.075 m^2 effective area parabolic mirror. In the present work, a 0.0615 m^2 area Fresnel lens was used to concentrate incoming solar power to a 2 mm diameter, 30 mm length Ce:Nd:YAG rod. 1.81 W continuous-wave 1064 nm solar laser output power was measured, corresponding to 3.15% solar-to-laser conversion efficiency, 4.4% laser slope efficiency, and 29.4 W/m^2 collection efficiency. More importantly, threshold incoming solar power as low as 16.5 W was achieved, representing a 3.33 times reduction in threshold solar power, as compared to previous record by the parabolic mirror. By using a 0.0855 m^2 area Fresnel lens, 2.83 W solar laser power was also measured, leading to 3.56% solar-to-laser conversion efficiency, 4.9% laser slope efficiency, and 33.1 W/m^2 collection efficiency. Low threshold incoming solar power of 22.7W was also obtained, representing a 2.42 times reduction in threshold solar power in relation to the previous record. Notably, 1.41 W TEM_{00} mode solar laser power was also measured by adopting an asymmetric laser resonant cavity, resulting in 2.06% solar-to-TEM_{00} mode laser conversion efficiency, which, to the best of our knowledge, is 2.61 times larger than the previous record by Nd:YAG medium.

1. Introduction

Solar-pumped laser can convert free solar radiation directly into coherent laser radiation without involving any electrical equipment. Solar laser technology is therefore very promising for space applications, like deep-space communication, laser power beaming, wireless solar power transmission from space to the Earth [1–3]. Cost effective generation of powerful coherent solar laser radiation can also be meaningful for terrestrial applications like material processing, renewable reduction of Mg from MgO [4,5], and wireless electric vehicle (EV) charging [6].

The first solar-pumped laser was reported by Kiss et al. and Young in the early 1960′s [7,8]. Considerable progresses in solar-to-laser conversion efficiency occurred in the last sixteen years, by pumping bulk Cr:Nd:YAG, Nd:YAG [9–15] and most recently Ce:Nd:YAG laser media [16–22]. The addition of the Ce^{3+} ion sensitizer into Nd^{3+}:YAG ensures an efficient absorption of the solar radiation in both ultraviolet (UV) and visible regions by Ce^{3+} ions, the energy of which is then transferred to Nd^{3+} ion [23], further increasing the number of Nd^{3+} ions in excited state. In 2021, Vistas et al. reported an improvement of 1.5 times in Ce:Nd:YAG rod solar laser efficiency over that with Nd:YAG rod under the same solar pumping conditions [17]. To significantly reduce the thermal load of Ce:Nd:YAG medium, Liang et al. used a three-rod configuration to simultaneously pump three thin Ce:Nd:YAG rods within a single cavity in 2022, attaining record-high solar laser collection and solar-to-laser conversion efficiencies of 41.25 W/m^2 and 4.64%, respectively [18]. Garcia et al. also utilized a parabolic mirror with 0.293 m^2 collection area to pump a single thin Ce:Nd:YAG rod with 2.5 mm diameter and 25 mm length [21]. 38.2 W/m^2 solar laser collection efficiency was measured. Moreover, 88 W threshold incoming solar power was found sufficient for initiating laser emission. Cai et al. used a 0.69 m^2 area Fresnel lens to pump a 6 mm diameter 95 mm length Ce:Nd:YAG/YAG grooved bonded crystal rod within a quartz cooling water tube and a gold-plated conical cavity in 2022 [22]. 3.85% solar-to-laser conversion efficiency and 38.8 W/m^2 collection efficiency were

* Corresponding author.
E-mail address: dl@fct.unl.pt (D. Liang).

https://doi.org/10.1016/j.solmat.2024.112817
Received 15 August 2023; Received in revised form 31 January 2024; Accepted 14 March 2024
Available online 19 March 2024

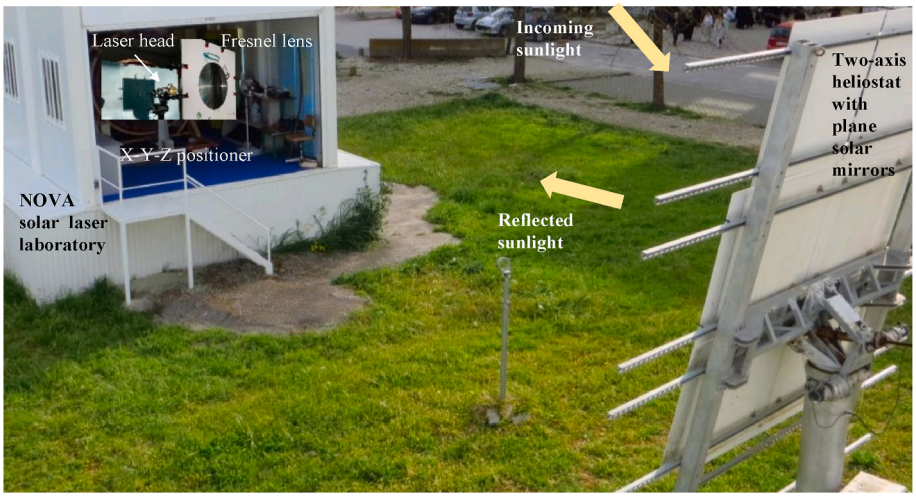

Fig. 1. Photograph of NOVA solar laser laboratory, which houses the Fresnel lens, the Ce:Nd:YAG laser head, and a X-Y-Z positioner. Additionally, a two-axis heliostat with plane solar mirrors located outside the laboratory was used to redirect incoming sunlight into the laboratory.

measured, respectively. However, threshold incoming solar power as high as 200 W was also registered.

On the one hand, despite the fact that it is now possible to attain successful laser emission without any solar concentrator and hence requiring the lowest threshold solar power [24], significant enhancement of solar-to-laser conversion efficiency is a must for this type of solar laser with transverse excitation fiber-laser geometry. On the other hand, despite the high solar-to-laser conversion efficiency of classical solar lasers with bulk active media, there is an urgent need to reduce their threshold incoming solar power so as to enable space and terrestrial applications. To reduce threshold incoming solar power for laser emission, 0.075 m^2 effective collection area of the medium size solar furnace (MSSF) of Procédés, Matériaux et Énergie Solaire—Centre National de la Recherche Scientifique (PROMES-CNRS) was used by Garcia et al. to end-side-pump a 2.5 mm diameter, 25 mm length Ce (0.1 at%): Nd (1.1 at%):YAG rod. Record low incoming solar power of 54.9 W was found for threshold solar laser operation [25].

TEM_{00} mode is one of the most preferred laser beam modes because of its smooth intensity profile, low divergence and ability to be focused to a diffraction-limited spot. The first TEM_{00} mode solar laser operation was obtained in 2013 by side-pumping a Nd:YAG rod [12]. The current record in solar-to-fundamental mode laser conversion efficiency was limited to 0.79%, obtained by using an end-side-pumping configuration and a Nd:YAG rod in 2017 [13]. Despite the significant enhancement in solar-to-multimode laser conversion efficiency by Ce:Nd:YAG medium [18], there was no report of significant improvement in solar-to-TEM_{00} mode laser conversion efficiency. The adoption of a small diameter Ce:Nd:YAG rod may considerably supress the oscillation of high-order laser mode and offer an effective solution in boosting this important efficiency. In this work, a lightweight and small area (0.0615 m^2) Fresnel lens was adopted as a primary solar concentrator to focus the incoming solar radiation, via a two-axis solar heliostat, to a 2 mm diameter, 30 mm length Ce:Nd:YAG rod, as shown in Fig. 1. Threshold incoming solar power as low as 16.5 W was found, representing 3.33 times reduction as compared to the previous record by the 0.075 m^2 parabolic mirror. More importantly, the use of the 2.0 mm diameter, 30 mm length Ce:Nd:YAG rod pumped through the 0.0855 m^2 area Fresnel lens produced 1.41 W TEM_{00} mode solar laser power. 2.06% solar power-to-TEM_{00} mode laser power conversion efficiency was successfully achieved, corresponding to 2.61 times improvement over the previous record from a 4.0 mm diameter, 35 mm length Nd:YAG rod [13]. Therefore, the combination of the small area Fresnel lens with the thin Ce:Nd:YAG rod can ensure a much easier and stable 1064 nm solar laser mission with the lowest threshold solar power, adequate for many potential applications.

2. NOVA Ce:Nd:YAG solar laser system pumped through the fresnel lens

As shown in Fig. 1, incoming sunlight was redirected to the Fresnel lens with 0.28 m (or 0.33 m) diameter, 600 mm focal length within NOVA solar laser laboratory by the two-axis heliostat with two planes solar mirrors (1.0 m × 1.4 m each). These mirrors were flat back-surface

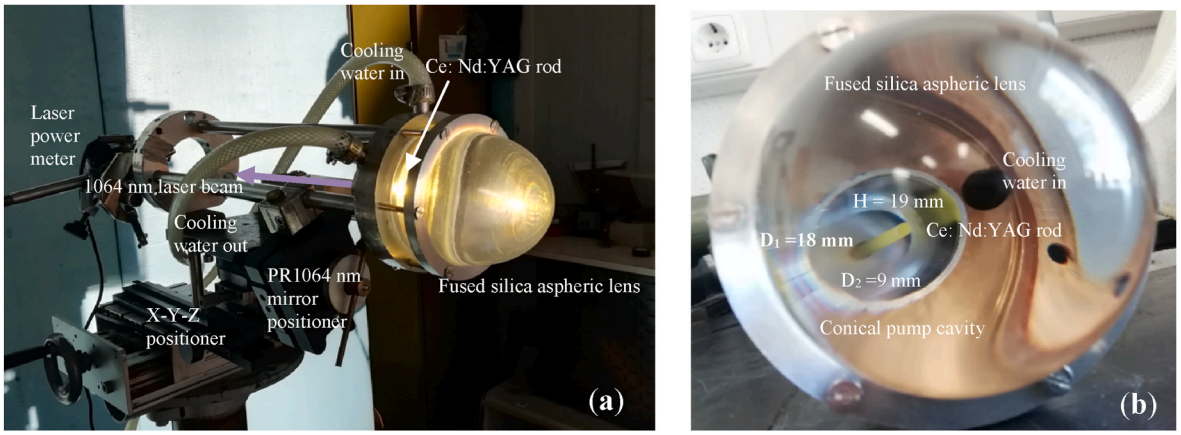

Fig. 2. Photograph of the solar laser head (a) housing the Ce:Nd:YAG crystal (b), placed at the focus of the 0.28 m Fresnel lens with 0.0615 m^2 collection area.

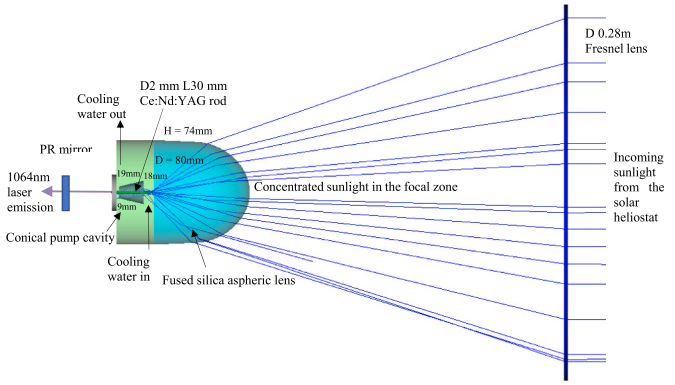

Fig. 3. Zemax© design of the solar laser head in end-side-pumping configuration, composed of the fused silica aspheric lens, the conical pump cavity, and the Ce:Nd:YAG laser rod actively cooled by water.

silver-coated mirrors and had a measured reflectivity of 92%. The Ce:Nd:YAG solar laser head was mounted onto a X-Y-Z mechanical positioner so as to achieve an accurate alignment in the focal zone of the Fresnel lens. A shutter (not shown in Fig. 1) was applied to control the solar power level reaching the Fresnel lens.

3. Ce:Nd:YAG solar laser head with an aspheric secondary concentrator

As shown in Figs. 2 and 3, the Ce:Nd:YAG solar laser head was composed of a large fused silica aspheric lens of 99.995% optical purity, so as to effectively focus the concentrated solar radiation from the Fresnel lens into the 2.0 mm diameter, 30 mm length Ce:Nd:YAG rod within the conical pump cavity.

The fused silica aspheric lens was 80 mm in diameter, 74 mm in height, 39 mm in front surface radius of curvature and - 0.003 in rear aspheric coefficient r^2 parameter. The output end face of the aspheric lens had a plane surface.

The Ce (0.1 at%):Nd (1.1 at%):YAG crystal was centered within a conical pump cavity covered with silver-coated aluminum foil of 94% reflectivity. The pump cavity had a conical shape with H = 19.0 mm length and input/output diameters of $D_1 = 18.0$ mm and $D_2 = 9.0$ mm, respectively, the dimensions of which were optimized numerically by Zemax© software. The conical pump cavity not only facilitated the easy flow of cooling water, but more importantly enabled efficient multi-pass side pumping of the laser rod, resulting in better pump energy absorption and distribution along the active medium. The Ce:Nd:YAG laser rod was cooled by water at 6 L/min flow rate. It had one end-face with a high-reflection (HR) coating at the laser emission wavelength (HR ≥ 99.5% @ 1064 nm), facing the output surface of the fused silica aspheric lens, while the other end-face had an anti-reflection (AR) coating with less than 0.2% reflectivity (AR≤0.2% @ 1064 nm). The active medium was acquired from Chengdu, Dongjun Laser Co., Ltd. (Chengdu, China). A partial-reflection (PR) coated output coupler for 1064 nm laser emission with either 97% or 98% reflectivity and a radius of curvature (RoC) of - 0.8 m was positioned 12 mm away from the AR coated end face of the Ce:Nd:YAG laser rod. The 1064 nm solar laser output power was measured by the Thorlabs PM1100D power meter, as indicated by Fig. 2a.

4. Numerical optimization of Ce:Nd:YAG solar laser design parameters by Zemax® and LASCAD™ software

Ce:Nd:YAG active media have revealed large capability to improve the broadband-pumped laser performance [16–22], as compared to the Nd:YAG media. Within the range of ultraviolet and blue wavelengths, the absorption of solar pump light by Ce^{3+} is strong and, most importantly, the energy transfer from Ce^{3+} to Nd^{3+} ions is efficient.

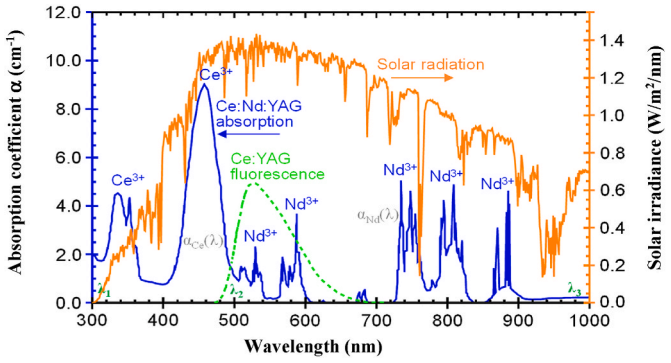

Fig. 4. Standard solar emission [26] (orange line), Ce^{3+} fluorescence (green line) and Ce^{3+}, Nd^{3+} absorption (blue line) spectra (adapted from Refs. [18,21], respectively).

The broad absorption bands centered at 339 nm and 460 nm correspond to transitions of the Ce^{3+} ions from the $2F_{5/2}$ ground state to the $5d_1$ and $5d_2$ excited states, respectively [27]. The other absorption bands at wavelengths greater than 500 nm are characteristic absorptions from the $^4I_{9/2}$ ground state of Nd^{3+} ions. The fluorescence of Ce^{3+} ions is characterized by a broad green-yellow (500–650 nm) emission band due to radiative decay from the 5d excited levels to the $^2F_{5/2}$ ground state [27], which overlaps well with the two green-yellow Nd^{3+} absorption bands at 515–540 nm and 565–595 nm. As shown in Fig. 4, 9.0 cm^{-1} is the highest absorption coefficient related to the Ce^{3+} absorption band at 460 nm, whereas the absorption coefficient of 4.5 cm^{-1} corresponds to the other Ce^{3+} ion band at 339 nm. The absorption coefficients of 586 nm and 531 nm Nd^{3+} ion peaks are 3.7 cm^{-1} and 2.3 cm^{-1}, respectively, while for the peaks at 880 nm, 865 nm, 808 nm, 793 nm, 746 nm, 736 nm, the Nd^{3+} ion absorption coefficients are 4.2 cm^{-1}, 3.1 cm^{-1}, 4.9 cm^{-1}, 4.2 cm^{-1}, 4.6 cm^{-1}, 5.0 cm^{-1}, respectively.

As indicated in Eq. (1), the total absorbed power ($P_{Nd^{3+}}$) per unit area can be calculated by introducing solar spectral irradiance I (λ), firstly from $\lambda_1 = 320$ nm to $\lambda_2 = 500$ nm to account for the solar power absorption by Ce^{3+} ions, and later from $\lambda_2 = 500$ nm to $\lambda_3 = 900$ nm to account for the absorption by Nd^{3+} ions. For the 0.1 at.% Ce^{3+}:1.1 at.% Nd^{3+}:YAG medium, the Ce^{3+} and Nd^{3+} ions absorption coefficients are denoted by $\alpha_{Ce}(\lambda)$ and $\alpha_{Nd}(\lambda)$, respectively.

$$P_{Nd^{3+}} = \int_{\lambda_1}^{\lambda_2} I(\lambda)[\,1 - \exp(-\alpha_{Ce}(\lambda)L)]\,\eta_{\text{non-radiative } Ce^{3+}-Nd^{3+}}\,d\lambda + \int_{\lambda_1}^{\lambda_2} I(\lambda)[\,1 - \exp(-\alpha_{Ce}(\lambda)L)]\,\eta_{\text{radiative } Ce^{3+}-Nd^{3+}}\,d\lambda + \int_{\lambda_2}^{\lambda_3} I(\lambda)[\,1 - \exp(-\alpha_{Nd}(\lambda)L)]\,d\lambda \quad (1)$$

The first and the second integrals of Eq. (1) represent the additional pathways of absorption for Nd^{3+} ions associated with the non-radiative and radiative energy transfer from Ce^{3+} to Nd^{3+} ions ($Ce^{3+} \rightarrow Nd^{3+}$), respectively, where $\eta_{\text{non-radiative } Ce^{3+}-Nd^{3+}}$ and $\eta_{\text{radiative } Ce^{3+}-Nd^{3+}}$ being the $Ce^{3+} \rightarrow Nd^{3+}$ non-radiative and radiative energy transfer efficiencies, respectively. Solar radiation direct absorption by Nd^{3+} ions is given by the third integral of Eq. (1). The effective absorption length within the laser medium is denoted by L and can be calculated by Zemax® analysis [18]. 15.3% overlap efficiencies between the solar emission and the Ce^{3+} absorption spectra, and 16.0% between the solar emission and Nd^{3+} absorption spectra were therefore calculated [18], confirming the 14%–16% solar emission and Nd^{3+} absorption spectral overlap of the previous literatures [14,28]. By taking into consideration a solar irradiance of 930 W/m^2, 0.0615 m^2 collection area, and 15.3 % overlap between the Ce^{3+} absorption and the AM1.5 solar emission spectra, an effective solar source power of 8.75 W was calculated for pumping the

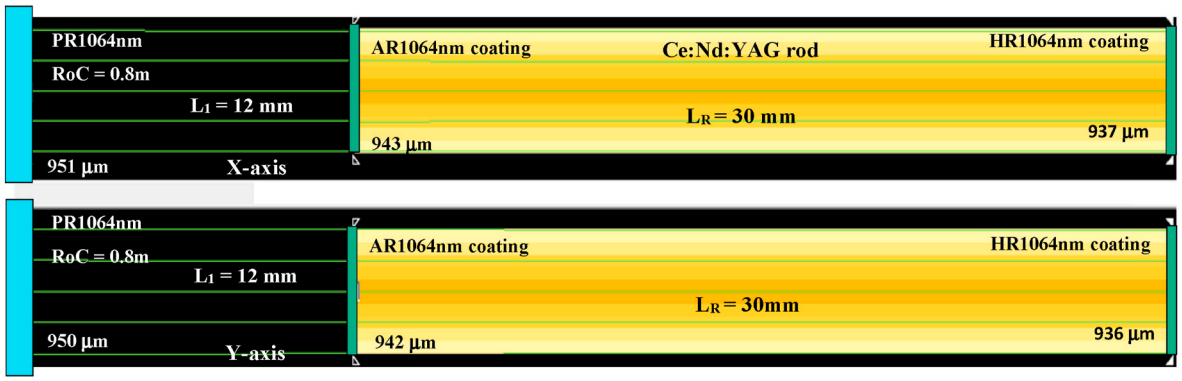

Fig. 5. Laser resonator configuration for the efficient extraction of multimode solar laser power from the Ce:Nd:YAG rod. L_1 represents the separation length between AR1064 nm and PR1064 nm coatings.

Ce^{3+} ions. Since non-radiative energy transfer efficiency from Ce^{3+} ions to Nd^{3+} ions of approximately 70% can occur [23], 8.75 W × 70% = 6.13 W source power was assigned to Source 1 in Zemax® software to calculate the effective absorbed pump power associated with the non-radiative Ce^{3+}→ Nd^{3+} transfer process. Moreover, considering an overlap efficiency of 16% between the Nd^{3+} ion absorption and the solar emission spectra, 9.15 W effective source power for direct pumping of the Nd^{3+} ions was added to Source 1. Consequently, total effective power of 15.28 W (6.13 W + 9.15 W) was assumed by considering the contributions of both Nd^{3+} absorption and Ce^{3+} absorption with the associated non-radiative energy transfer from Ce^{3+} to Nd^{3+}. In Zemax® software, Source 1 was composed of 16 narrow Nd^{3+} ion absorption wavelengths centered at 880 nm, 865 nm, 820 nm, 815 nm, 808 nm, 805 nm, 803 nm, 793 nm, 790 nm, 758 nm, 753 nm, 746 nm, 743 nm, 736 nm, 732 nm, 592 nm, 586 nm, 579 nm, 569 nm, 531 nm, and 527 nm.

Besides, about 30% of the absorbed solar energy by Ce^{3+} ion can be radiated in the form of green-yellow color fluorescence, which can consequently be absorbed by the Nd^{3+} ion due to the six Nd^{3+} absorption wavelengths centered at 592 nm, 586 nm, 579 nm, 569 nm, 531 nm, and 527 nm [18], an effective source power of 57.2W × 15.3% × 30% = 2.63 W was hence attributed to Source 2 in Zemax® analysis. Additionally, the weight of each absorption peak of Source 2 was determined using the fluorescence irradiance value $I_f(\lambda)$ for the corresponding peak wavelength λ [18].

Finally, the Ce:Nd:YAG solar laser numerical optimization process was initiated in a way similar to our previous numerical analysis on solar lasers [10,12,13,15–21]. All the above mentioned laser design parameters in Section 3 were optimized by non-sequential ray-tracing Zemax® software for achieving the maximum effective absorbed solar pump power for the 2 mm diameter, 30 mm length Ce:Nd:YAG laser rod. 92% heliostat plane mirror reflectivity was considered in Zemax® analysis.

The absorbed pump flux data containing 62500 zones from the Zemax® analysis was processed by laser cavity analysis and design (LASCAD™) software to optimize solar laser output performances. The stimulated emission cross-section of 2.8×10^{-19} cm^2, the fluorescence lifetime of 230 μs, and the absorption and scattering loss of 0.003 cm^{-1} for the 0.1 at.% Ce: 1.1 at.% Ce:Nd:YAG rod were used in LASCAD™ analysis. The mean absorbed and intensity-weighted solar pump wavelength of 660 nm [28] was included in the analysis. The separation length L_1 between the output end face anti-reflection (AR) 1064 nm coatings of the Ce Nd:YAG rod and PR1064 nm output mirror was 12 mm, as shown in Fig. 5. More importantly, PR1064 nm output mirrors of different reflectivity (R) and RoC were tested to optimize the laser power from the Ce:Nd:YAG rod.

For the 2.0 mm diameter, 0.1 at.% Ce:1.1 at.% Nd:YAG rod with length $L_R = 30$ mm, the amount of absorption and scattering losses was $2\alpha L_R = 1.8\%$. Assuming 0.7% of imperfect HR and AR coating losses, the total round-trip loss was increased to 2.5%. The laser resonant cavity diffraction losses depend strongly on rod diameter, resonator length, and RoC of the resonator mirrors. LASCAD™ beam propagation method gave negligible diffraction loss for RoC = 0.8 m, resulting in a total round-trip loss of 2.5%. Consequently, 1.81 W maximum multimode laser power was numerically calculated by LASCAD™ software. As shown in Fig. 5, the half-width of laser oscillating mode within the laser resonant cavity was also calculated, being 937 μm in X-axis and 936 μm in Y-axis at HR1064 nm mirror, 943 μm in X-axis and 942 μm in Y-axis at AR1064 nm mirror and 951 μm in X-axis, 950 μm in Y-axis at PR1064 nm mirror.

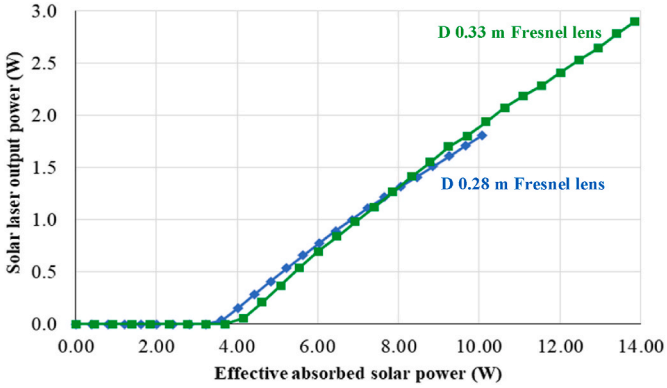

Fig. 6. Numerically calculated laser power versus effective absorbed solar pump power from the 2.0 mm diameter, 30 mm length Ce:Nd:YAG rod pumped through the 0.28 m, 0.33 m diameter Fresnel lens, respectively.

In Fig. 6, blue line shows the relation between multimode laser output power and effective absorbed solar pump power when the 0.28 m diameter, 0.6 m focal length Fresnel lens was used to pump the 2 mm diameter Ce:Nd:YAG rod. 1.81 W maximum solar laser output power was numerically obtained for 10.06 W effective absorbed solar pump power. 3.0 W effective threshold absorbed power was found sufficient for initiating the lasing process. The laser beam quality factors of $M_x^2 = M_y^2 = 25$ were numerically obtained by LASCAD™ beam propagation method (BPM) analysis for the PR1064 nm mirror with RoC = 0.8 m. In Fig. 6, green line shows the relation between multimode laser power and absorbed solar pump power when the 0.33 m diameter, 0.6 m focal length Fresnel lens was used to pump the same Ce:Nd:YAG rod. 2.83 W maximum solar laser output power was numerically obtained for 14.0 W effective absorbed solar power. 4.0 W effective threshold absorbed solar power was calculated. The laser beam quality factors of $M_x^2 = M_y^2 = 23.6$ were also numerically obtained by LASCAD™ BPM analysis for the PR1064 nm mirror with RoC = 0.8 m.

As shown in Fig. 7, the heat load, temperature, and stress intensity of

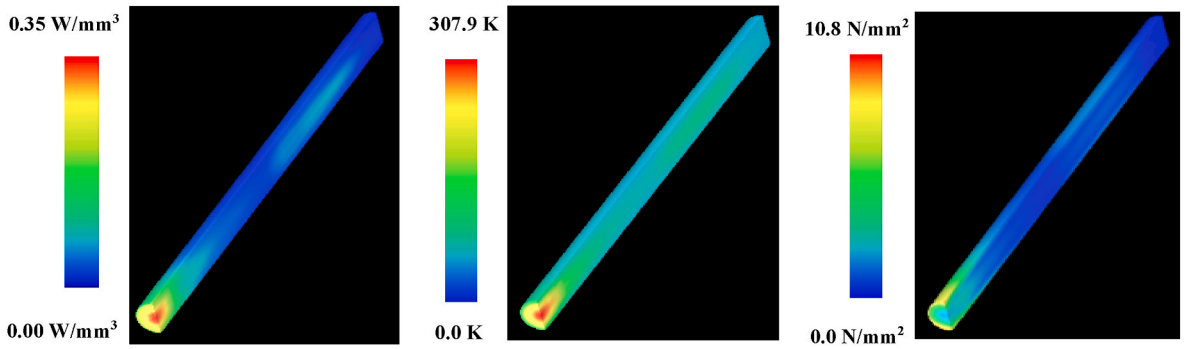

Fig. 7. Heat load, temperature and stress intensity of the 2.0 mm diameter, 30 mm length Ce:Nd:YAG rod, numerically calculated by LASCAD™ analysis.

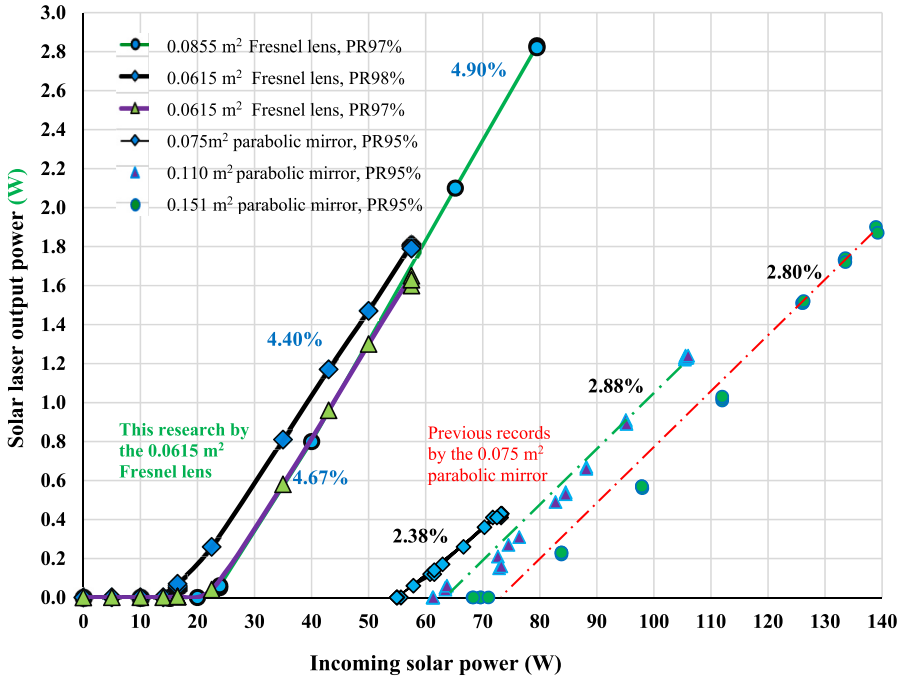

Fig. 8. Solar laser output power versus incoming solar power and their respective slope efficiencies. Previous records by the parabolic mirror are also listed.

the 2.0 mm diameter, 30 mm length Ce:Nd:YAG rod was numerically calculated through LASCAD™ analysis. The Ce:Nd:YAG solar laser presented only 0.35 W/mm^3 maximum heat load, 307.9 K maximum temperature, and 10.8 N/mm^2 maximum thermal stress values, which are substantially lower than that of most recent Fresnel lens single Ce:Nd:YAG solar laser pumping scheme [22], ensuring consequently enhanced laser output beam stability and laser efficiency according to Payziyev et al.'s analysis [29].

5. Lowest-threshold continuous-wave solar laser emission from the Ce:Nd:YAG rod

Based on the numerically optimized design parameters of the Ce:Nd:YAG rod solar laser system by Zemax® and LASCAD™ software, a solar laser prototype was firstly designed and built in 2022, and secondly tested in both the PROMES–CNRS and the NOVA solar facilities in 2023, as shown in Fig. 1.

Continuous-wave 1064 nm solar laser beam emissions were successfully obtained from the Ce:Nd:YAG rod in both solar facilities, attaining the highest solar-to-laser conversion efficiency in the NOVA solar facility in May 2023. The data acquisition process consisted of the registration of the laser output power as a function of the incoming solar power, which was controlled by the shutter (not shown in Fig. 1). As shown in Fig. 8, under clear sky condition with 930 W/m^2 solar irradiance, when a 98% PR1064 nm output mirror with 0.8 m RoC was used, solar laser emission was firstly spotted with the shutter opened at 28.7% for 0.0615 m^2 collection area, corresponding to 16.5 W corresponding to 16.5 W threshold incoming solar power.

By fully opening the shutter, maximum solar laser output powers of 1.81 W was measured with solar power of 57.4 W, corresponding to 3.15% solar-to-laser conversion efficiency, 4.40% laser slope efficiency, and 29.4 W/m^2 collection efficiency. With a 97% PR1064 nm output mirror with 0.8 m RoC, under clear sky condition at an average solar irradiance of 930 W/m^2, solar laser emission was observed with the shutter opened at 39.1% for 0.0615 m^2 collection area, corresponding to 22.5 W threshold incoming solar power. By fully opening the shutter, maximum solar laser output power of 1.63 W was measured with incoming solar power of 57.4 W, corresponding to 2.84% solar-to-laser conversion efficiency, 4.67% laser slope efficiency, and 26.5 W/m^2 collection efficiency.

As shown in Fig. 8, by using the 0.33 m diameter Fresnel lens with 0.0855 m^2 collection area and a 97% PR1064 nm output mirror with 0.8 m RoC, also under clear sky condition with an average solar irradiance of 930 W/m^2, 2.83 W continuous-wave 1064 nm solar laser power was

Table 1
Progress in Ce:Nd:YAG solar laser threshold power and efficiency.

Sky status	Clear	Clear	Improvement (times)	Clear	Improvement (times)
Date	September 2022	May 2023		May 2023	
Primary concentrator	Parabolic mirror (PROMES) 0.075 m^2	Fresnel lens (**D0.28m**) 0.0615 m^2		Fresnel lens (**D0.33m**) 0.0855 m^2	
Total reflectivity of the collection system	59%	92% (heliostat mirror)		92% (heliostat mirror)	
Effective collection area	0.075 m^2	0.0615 m^2		0.0855 m^2	
Tracking method	Via heliostat	Via heliostat		Via heliostat	
Active medium	Ce:Nd:YAG	Ce:Nd:YAG		Ce:Nd:YAG	
Pumping method	end-side-pumping	end-side-pumping		end-side-pumping	
Laser rod dimensions	Ø 2.5 mm × 25 mm	Ø 2.0 mm × 30 mm		Ø 2.0 mm × 30 mm	
Solar irradiance	916-927 W/m^2	930 W/m^2		930 W/m^2	
Maximum incoming solar power	73.2W	57.4 W		79.5 W	
Maximum laser power	0.42 W	1.81 W		2.83 W	
Threshold incoming solar power	54.9 W	**16.5 W**	**3.33 times reduction**	**22.7 W**	**2.42 times reduction**
Slope efficiency	2.38%	4.4%	**1.85**	4.9%	**2.06**
Solar-to-laser conversion efficiency	0.97%	3.15%	**3.25**	3.56%	**3.67**
Solar collection efficiency	5.57 W/m^2	29.4 W/m^2	**5.28**	33.1 W/m^2	**5.94**

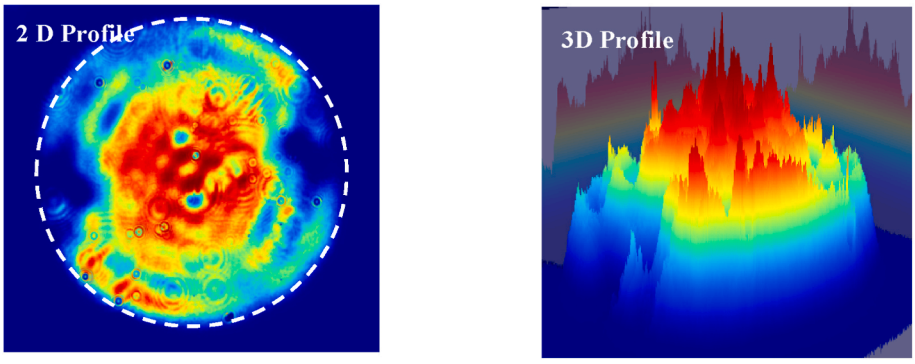

Fig. 9. Measured 2D and 3D beam profiles of the Ce:Nd:YAG solar laser beam, 320 mm away from the PR1064nm output mirror.

measured, leading to 3.56% solar-to-laser conversion efficiency, 4.9% laser slope efficiency, and 33.1 W/m^2 collection efficiency, revealing a large advantage in relation to that of the 0.075 m^2 parabolic mirror. Threshold incoming solar pump power of 22.7 W was attained, representing 2.42 times reduction in incoming threshold solar power, as compared to that by the 0.075 m^2 parabolic mirror.

To facilitate an easier comparison, previous records with the 0.075 m^2 parabolic mirror, in terms of threshold incoming solar power of 68.1 W, 61.2 W, and 54.9 W, as well as their corresponding maximum solar laser output power of 1.94 W, 1.24 W, and 0.43 W, respectively, were also provided in Fig. 8.

Table 1 compares the threshold incoming solar power of present Ce:Nd:YAG solar laser with the Fresnel lenses and the previous records with the 0.075 m^2 parabolic mirror. Solar laser slope efficiency, the solar-to-laser power conversion, and the solar laser collection efficiencies comparison were also listed.

Finally, multimode laser beam profile was measured by using a CINOGY UV-NIR beam profiler - CinCam CMOS positioned 5 mm, 320 mm away from the output end face of the rod. Slight discrepancies of laser beam profile in X and Y axis were observed, as shown in Fig. 9.

For laser beam quality M2 factors measurement, a 10" x 10" industrial standard laser alignment thermal sensitive paper ZAP-IT@ was positioned 320 mm away from the output coupler. The laser beam divergence θ was found by adopting Eq. (2):

$$Tan\,\theta = \frac{\varnothing_2 - \varnothing_1}{2\,L} \tag{2}$$

where $\varphi_1 = 1.9$ mm and $\varphi_2 = 7.0$ mm were the measured laser beam diameters, detected 5 mm and 330 mm away from the output mirror, respectively, and L was the distance between these two points. θ = 0.464° was calculated by Eq. (2).

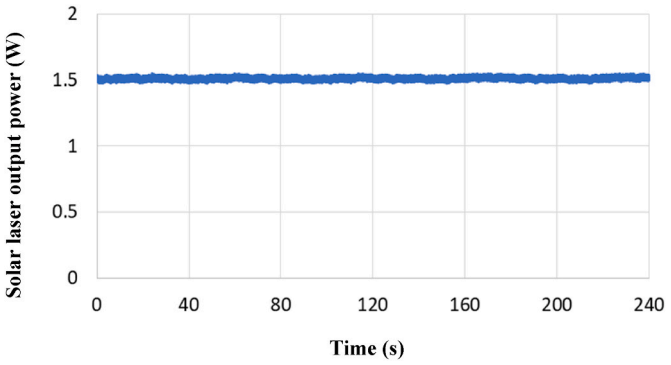

Fig. 10. Solar laser output power versus time of measurement.

M^2 factor was then calculated by Eq. (3):

$$M^2 = \frac{\vartheta}{\theta_0} \tag{3}$$

where $\theta_0 = \frac{\lambda}{\pi\omega_0} = 0.02°$ was the divergence of diffraction-limited Gaussian beam for $\lambda = 1.064$ μm and $\omega_0 = 950$ μm, as calculated by LASCAD™ laser beam propagation method for the 2 mm diameter rod in Fig. 5. For - 0.8 m RoC output coupler, $M_x^2 = M_y^2 = 23.2 \pm 5\%$ were experimentally determined. It is important to note that the measured laser beam quality M^2 factors were close to the numerical predicted value of $M_x^2 = M_y^2 = 25.0$ by LASCAD™ software.

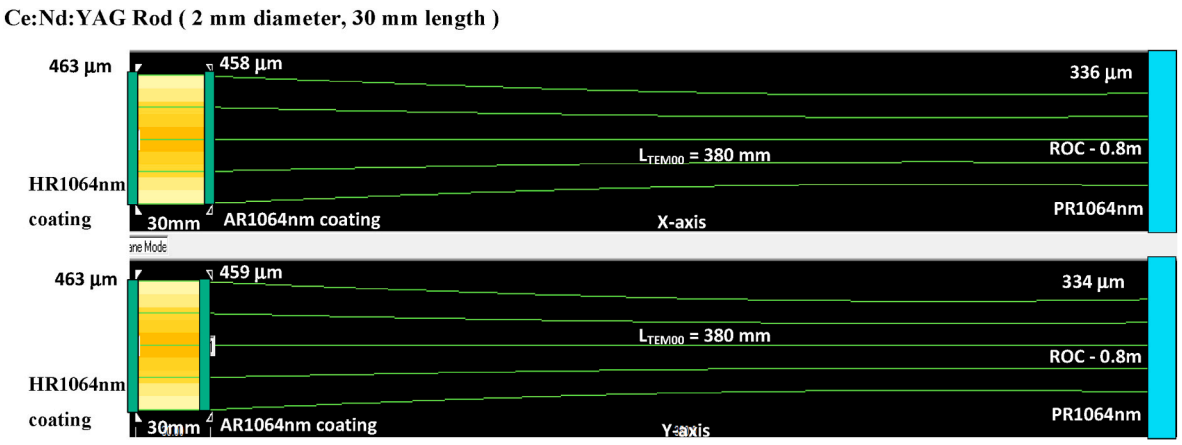

Fig. 11. Asymmetric laser resonator configuration for the efficient extraction of TEM_{00} mode solar laser power from the Ce:Nd:YAG rod. L_{TEM00} represents the separation length between the AR1064 nm coating and the PR1064 nm mirror.

6. Ce:Nd:YAG solar laser output power stability measurement

There are many factors causing solar laser output power fluctuation, including solar pump power fluctuation, cooling temperature drift, crystal temperature change and mechanical structure instability of the Ce:Nd:YAG solar laser. To eliminate the influence of solar irradiance variation along the day, solar laser power measurement interval was limited to less than 240 s. Ce:Nd:YAG solar laser output power were registered, several times, during each 240 s period, between 12h and 13h on 14th of December 2023. 810 W/m^2 solar irradiance was measured and remained nearly constant during each period of 240 s. In Fig. 10 is shown how the multimode solar laser output power with 1.51W average value typically varied during the measurement. As given by Eq. (4), peak-to-peak laser power stability is defined as the difference between the maximum and minimum values of output power and the percentage of the average power value, representing the range of output power variation within a given time.

$$\sigma = \frac{(P_{max} - P_{min})/2}{\left(\sum_{i=1}^{N} P_i\right)\Big/ N} \times 100\% \quad (4)$$

From the laser output data in Fig. 10, solar laser beam stability of σ = 1.1 % was calculated. Indeed, the adoption of the thin and long (2 mm diameter, 30 mm length) Ce:Nd:YAG rod, efficiently cooled by water, and pumped by low incoming solar power contributed significantly to the good solar laser output power stability in Fig.10.

7. Most-efficient TEM_{00} mode continuous-wave Ce:Nd:YAG solar laser emission

7.1. LASCAD™ numerical analysis of TEM_{00} mode laser power and beam profile

For the 0.33 m diameter Fresnel lens with 0.0855 m^2 effective collection area and 800 W/m^2 solar irradiance on 1st of January 2023 in Lisbon area, the NOVA heliostat-parabolic mirror system collected about 45 W solar powers to its focal zone.

Similar to the numerical analysis in multimode regime in Section 4, all the TEM_{00} mode Ce:Nd:YAG solar laser design parameters were optimized by non-sequential ray-tracing Zemax® software for achieving the maximum absorbed solar pump power by the 2 mm diameter, 30 mm length Ce:Nd:YAG rod. The optimized absorbed pump flux data containing 62500 zones from the Zemax® analysis was then processed by LASCAD™ software to analyze the solar laser output performance in TEM_{00} mode regime. The TEM_{00} mode laser output power and beam profile at different L_{TEM00} were numerically optimized by LASCAD™ software. As mentioned in Section 4, PR1064 nm output mirrors of different reflectivity and RoC were used to optimize the fundamental solar laser power from the Ce:Nd:YAG rod. As indicated by Fig. 7, the Ce:Nd:YAG rod was subjected to 0.35 W/mm^3 maximum heat load, 307.9 K maximum temperature and 10.8 N/mm^2 maximum thermal stress values, which determined the thermal focal length L_{TEM00} in LASCAD™ fundamental mode laser power and beam quality M^2 factor analysis. For TEM_{00} mode laser oscillation, in LASCAD™ software, the asymmetric laser resonator was adopted because it provides a large spatial overlap between the fundamental laser mode volume and solar pump volume, improving thus the laser output performance. Thermal focal length L_{TEM00} was a key parameter to achieve the optimum mode overlap. To obtain efficient extraction of fundamental mode power, the TEM_{00} mode laser usually operate near the edge of the optically stable region. As shown in Fig. 11, the half-width of the laser oscillating mode within the laser resonant cavity were numerically calculated, being 463 µm in X-axis and 464 µm in Y-axis at HR1064 nm coating, 458 µm in X-axis and 459 µm in Y-axis at AR1064 nm coating, and 336 µm in X-axis, 334 µm in Y-axis at PR1064 nm output mirror. For TEM_{00} mode laser oscillation, the - 0.8 m RoC output mirror with 97% reflectivity at L_{TEM00} = 380 mm were found to offer the maximum TEM_{00} mode laser output power of 1.47 W and laser beam quality factor M_x^2 = 1.00, M_y^2 = 1.07 were also numerically calculated by LASCAD™ software.

7.2. Continuous-wave TEM_{00} mode Ce:Nd:YAG solar laser emission experiment

In fundamental mode laser oscillation experiment, the - 0.8 m RoC output mirror with 97% reflectivity at L_{TEM00} = 380 mm thermal focal length offered the maximum TEM_{00}-mode laser output power of 1.41 W, as shown in Fig. 13, when pumped by the maximum incoming solar power of 68.4 W, which matched well with the LASCAD™ numerical analyses.

For the 0.33 m diameter Fresnel lens with 0.0855 m^2 collection area and 800 W/m^2 solar irradiance, 68.4 W incoming solar power was calculated. 1.41W TEM_{00} mode solar laser power was measured by placing the laser power meter directly after the 97% PR1064nm output coupler. 2.06% solar-to-TEM_{00} mode laser conversion efficiency was calculated, which is 2.61 times higher than the previous record by using Nd:YAG medium [13].

As shown in Fig. 13, a CINOGY UV-NIR beam profiler - CinCam CMOS was placed 430 mm away from the AR1064nm end face of the Ce:Nd:YAG rod in order to avoid damaging its CMOS detector by high brightness fundamental mode solar laser beam. To measure the beam diameters at 1/e^2 width under extremely high 1064 nm laser radiation, another 95% 1064 nm ROC = ∞ output mirror was added before the

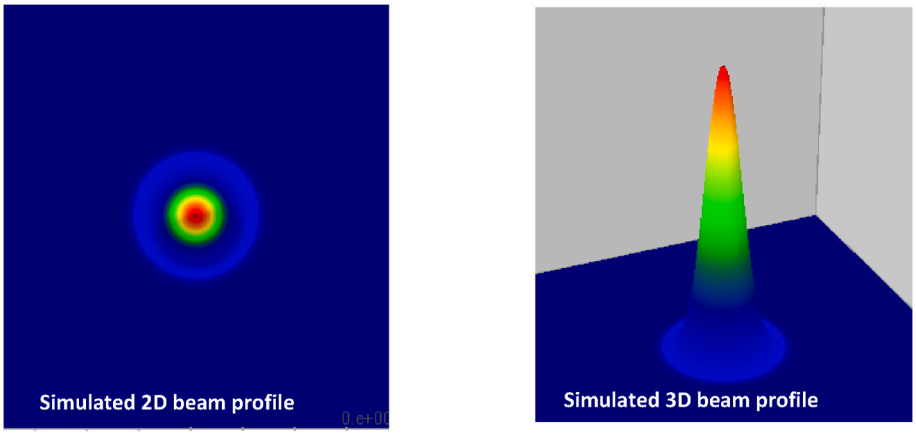

Fig. 12. Numerically simulated 2D and 3D beam profiles of the Ce:Nd:YAG solar laser beam. The PR1064 nm output mirror was positioned $L_{TEM00} = 380$ mm away from the AR1064 coating of the Ce:Nd:YAG laser rod.

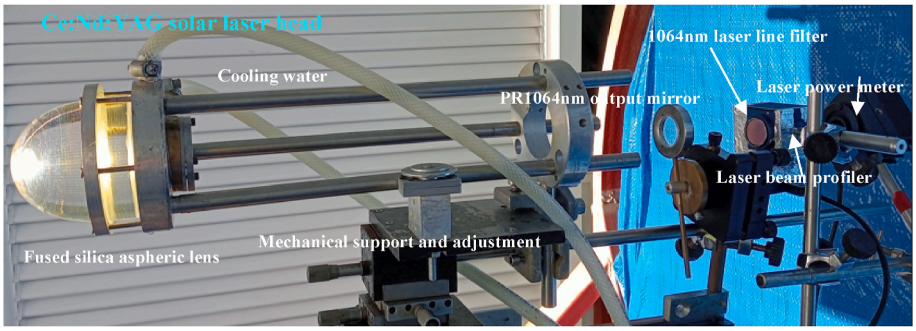

Fig. 13. Ce:Nd:YAG solar laser head for the efficient extraction of 1.41 W continuous-wave TEM_{00} mode solar laser power.

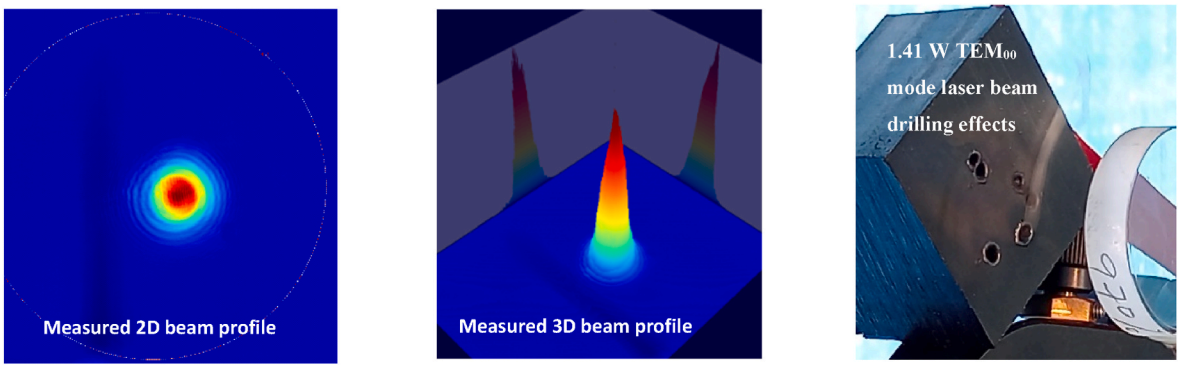

Fig. 14. (a), (b) Measured TEM_{00} mode output laser beam 2D and 3D profiles 60 mm away from the PR1064 nm mirror. (c) 1.41W TEM_{00} mode solar laser beam drilling effect 20 mm away from the 97% 1064 nm output mirror. 1.41W TEM_{00} mode solar laser power was also measured by placing the laser power meter directly after the 97% PR1064 nm output mirror.

CMOS detector, acting as an extra laser beam attenuator and reducing the 1064 nm laser power level only mW before reaching the CMOS detector. A 05LF10-1064 laser line filter was also mounted on the entrance window of the CINOGY beam profiler to identify the laser emission wavelength. This laser line filter had the center wavelength of 1064 ± 2 nm, and full width half max of 10 ± 2 nm. The laser line filter was ideal for transmitting 1064 nm laser light while suppressing ambient light for the profiler. The highly reflective side of the filter was positioned to face the incoming laser beam. 79% transmission efficiency for 1064 nm laser line was measured for this filter.

Measured TEM_{00} mode output laser beam 2D and 3D profiles 60 mm away from the PR1064 nm mirror are shown by Fig. 14 (a) and (b). $M_x^2 \approx M_y^2 \leq 1.08$ were estimated. Finally, from Figs. 12 and 14, it is important to note the good agreement between the numerically calculated and the measured laser output beam profiles, as well as the effectiveness of the 1.41 W continuous-wave fundamental mode solar laser beam for high quality laser material processing applications.

8. Conclusions

By using the 0.28 m diameter Fresnel lens with 0.0615 m^2 collection area, at an average solar irradiance of 930 W/m^2, 1.81 W continuous-wave 1064 nm solar laser power was measured, leading to 3.15% solar-to-laser conversion efficiency, 4.4% laser slope efficiency, and 29.4 W/m^2 collection efficiency, revealing clear efficiency advantages in relation to that of the 0.075 m^2 parabolic mirror. More importantly,

threshold incoming solar power of 16.5 W was successfully achieved, representing a 3.33 times reduction in threshold solar pump power, as compared to that with the 0.075 m^2 parabolic mirror. By using the 0.33 m diameter Fresnel lens with 0.0855 m^2 collection area with an average solar irradiance of 930 W/m^2, 2.83 W continuous-wave 1064 nm solar laser power was measured, leading to 3.56% solar-to-laser conversion efficiency, 4.9% laser slope efficiency, and 33.1 W/m^2 laser collection efficiency, revealing a large efficiency advantage in relation to that of the 0.075 m^2 parabolic mirror. Threshold incoming solar pump power of 22.7 W was successfully measured, representing a 2.42 times reduction in threshold incoming solar pump power, as compared to that by the 0.075 m^2 parabolic mirror. Due to the use of solar heliostat, the continuous-wave 1064 nm solar laser emission from the Ce:Nd:YAG rod was both stationary and stable. Due to the significant reduction in threshold solar power level, this laser also worked successfully in cloudy sky condition, as happened with our previous Ce:Nd:YAG solar laser prototype pumped through the 0.075 m^2 parabolic mirror [25]. Most notably, the adoption of the 2 mm diameter, 30 mm length Ce:Nd:YAG rod enabled the successful emission of 1.41W continuous-wave TEM_{00} mode solar laser power, surpassing the previous solar-to-fundamental mode laser conversion efficiency by 2.61 times. Therefore, the combination of the small diameter Fresnel lens with the small diameter Ce:Nd:YAG rod may contribute considerably in wide-spreading the application fields of solar-powered lasers, such as renewable light energy storage and H_2 production [30–32].

CRediT authorship contribution statement

Dawei Liang: Writing – review & editing, Writing – original draft, Validation, Supervision, Resources, Project administration, Methodology, Investigation, Funding acquisition, Conceptualization. **Joana Almeida:** Writing – review & editing, Investigation, Funding acquisition, Data curation. **Miguel Catela:** Writing – review & editing, Investigation, Data curation. **Hugo Costa:** Writing – review & editing, Investigation, Data curation. **Dário Garcia:** Writing – review & editing, Software, Data curation. **Bruno D. Tibúrcio:** Writing – review & editing, Data curation. **Emmanuel Guillot:** Resources, Investigation, Funding acquisition. **Cláudia R. Vistas:** Writing – review & editing, Software, Data curation.

Declaration of competing interest

Regarding to our manuscript entitled “Lowest-threshold Ce:Nd:YAG solar laser operation by a small area Fresnel lens” submitted to Solar Energy Materials and Solar Cells, we declare that there is no conflict of interest regarding the publication of this paper. The mentioned received funding in the "Acknowledgment" section did not lead to any conflict of interests regarding the publication of this manuscript.

Data availability

Data will be made available on request.

Acknowledgments

Financial support of the strategic project (UIDB/00068/2020) of the Science and Technology Foundation of the Portuguese Ministry of Science, Technology and Higher Education (FCT – MCTES) is acknowledged. Financial support by the Solar Facilities for European Research Area – Third Phase (SFERA III), Grant Agreement No. 823802 is gratefully acknowledged. The FCT-MCTES fellowship grants PD/BD/142827/2018, SFRH/BPD/125116/2016, SFRH/BD/145322/2019, 2021.06172.BD of D. Garcia, C. R. Vistas, M. Catela, H. Costa, respectively, and the Contract CEECIND/03081/2017 of J. Almeida are all acknowledged.

References

[1] L. Mordechai, A.K. Jacob, S. Yehoshua, Y.K. Yehoshua, N. Yoram, Y. Amnon, R. R. Stanley, R. Salman, Solar-pumped solid state laser program, Proc. SPIE 3110 (1997) 196–201. https://ui.adsabs.harvard.edu/abs/1997SPIE.3110..196L/abstract.

[2] M. Vasile, C.A. Maddock, Design of a formation of solar pumped lasers for asteroid deflection, Adv. Space Res. 50 (7) (2012) 891–905, https://doi.org/10.1016/j.asr.2012.06.001.

[3] Y. Abdel-Hadi, Space-based solar laser system simulation to transfer power onto the earth, NRIAG J. Astron. Geophys. 9 (1) (2020) 558–562. https://doi:10.1080/20909977.2020.1815497.

[4] T. Yabe, S. Uchida, K. Ikuta, K. Yoshida, C. Baasandash, M.S. Mohamed, Y. Sakurai, Y. Ogata, M. Tuji, Y. Mori, Y. Satoh, T. Ohkubo, M. Murahara, A. Ikesue, M. Nakatsuka, T. Saiki, S. Motokoshi, C. Yamanaka, Demonstrated fossil-fuel-free energy cycle using magnesium and laser, Appl. Phys. Lett. 89 (26) (2006) 261107. http://doi:10.1063/1.24233202022.

[5] T. Yabe, B. Bagheri, T. Ohkubo, S. Uchida, K. Yoshida, T. Funatsu, T. Oishi, K. Daito, M. Ishioka, N. Yasunaga, Y. Sato, C. Baasandash, Y. Okamoto, K. Yanagitani, 100 W-class solar pumped laser for sustainable magnesium-hydrogen energy cycle, J. Appl. Phys. 104 (8) (2008) 083104. http://doi:10.1063/1.2998981.

[6] T. Motohiro, Y. Takeda, H. Ito, K. Hasegawa, A. Ikesue, T. Ichikawa, K. Higuchi, A. Ichiki, S. Mizuno, T. Ito, N. Yamada, H.N. Luitel, T. Kajino, H. Terazawa, S. Takimoto, K. Watanabe, Concept of the solar-pumped laser-photovoltaics combined system and its application to laser beam power feeding to electric vehicles, Jpn. J. Appl. Phys. 56 (8S2) (2017) 08MA07. http://doi:10.7567/JJAP.56.08MA07.

[7] Z.J. Kiss, H.R. Lewis, R.C. Duncan, Sun pumped continuous optical maser, Appl. Phys. Lett. 2 (5) (1963) 93–94, https://doi.org/10.1063/1.1753794.

[8] C.G. Young, A sun pumped cw one-watt laser, Appl. Opt. 5 (1966) 993–997, https://doi.org/10.1364/AO.5.000993.

[9] T. Yabe, T. Ohkubo, S. Uchida, K. Yoshida, M. Nakatsuka, T. Funatsu, A. Mabuti, A. Oyama, K. Nakagawa, T. Oishi, K. Daito, B. Behgol, Y. Nakayama, M. Yoshida, S. Motokoshi, Y. Sato, C, Baasandash, High-efficiency and economical solar-energy-pumped laser with Fresnel Lens and chromium codoped laser medium, Appl. Phys. Lett. 90 (26) (2007) 261120, https://doi.org/10.1063/1.2753119, 2007.

[10] D. Liang, J. Almeida, Highly efficient solar-pumped Nd:YAG laser, Opt Express 19 (2011) 26399–26405, https://doi.org/10.1364/OE.19.026399.

[11] T.H. Dinh, T. Ohkubo, T. Yabe, H. Kuboyama, 120 watt continuous wave solar-pumped laser with a liquid light-guide lens and a Nd:YAG rod, Opt. Lett. 37 (2012) 2670–2672, https://doi.org/10.1364/OL.37.002670.

[12] D. Liang, J. Almeida, Solar-pumped TEM_{00} mode Nd:YAG laser, Opt Express 21 (2013) 25107–25112. https://opg.optica.org/oe/fulltext.cfm?uri=oe-21-21-25107&id=268986.

[13] D. Liang, J. Almeida, C.R. Vistas, E. Guillot, Solar-pumped Nd:YAG laser with 31.5 W/m^2 multimode and 7.9 W/m^2 TEM_{00}-mode collection efficiencies, Sol. Energy Mater. Sol. Cells 159 (2017) 435–439, https://doi.org/10.1016/j.solmat.2016.09.

[14] Z. Guan, C. Zhao, J. Li, D. He, H. Zhang, 32.1 W/m^2 continuous wave solar pumped laser with a bonding Nd:YAG/YAG rod and a Fresnel lens, Opt Laser. Technol. 107 (2018) 158–161, https://doi.org/10.1016/j.optlastec.2018.05.039.

[15] D. Liang, C.R. Vistas, B.D. Tíbúrcio, J. Almeida, Solar-pumped Cr:Nd:YAG ceramic laser with 6.7% slope efficiency, Sol. Energy Mater. Sol. Cells 185 (2018) 75–79, https://doi.org/10.1016/j.solmat.2018.05.020.

[16] C.R. Vistas, D. Liang, D. Garcia, J. Almeida, B.D. Tibúrcio, E. Guillot, Ce:Nd:YAG continuous-wave solar-pumped laser, Optik 207 (2020) 163795, https://doi.org/10.1016/j.ijleo.2019.163795.

[17] C.R. Vistas, D. Liang, J. Almeida, B.D. Tibúrcio, D. Garcia, M. Catela, H. Costa, E. Guillot, Ce:Nd:YAG side-pumped solar laser, J. Photonics Energy 11 (1) (2021) 018001, https://doi.org/10.1117/1.JPE.11.018001.

[18] D. Liang, C.R. Vistas, D. Garcia, B.D. Tibúrcio, M. Catela, H. Costa, E. Guillot, J. Almeida, Most efficient simultaneous solar laser emissions from three Ce:Nd:YAG rods within a single pump cavity, Sol. Energy Mater. Sol. Cells 246 (1) (2022) 111921, https://doi.org/10.1016/j.solmat.2022.111921.

[19] J. Almeida, D. Liang, D. Garcia, B.D. Tibúrcio, H. Costa, M. Catela, E. Guillot, C. R. Vistas, 40 W continuous wave Ce:Nd:YAG solar laser through a fused silica light guide, Energies 15 (11) (2022) 3998. https://doi:10.3390/en15113998.

[20] C.R. Vistas, D. Liang, D. Garcia, M. Catela, B.D. Tibúrcio, H. Costa, E. Guillot, J. Almeida, Uniform and non-uniform pumping effect on Ce:Nd:YAG side-pumped solar laser output performance, Energies 15 (10) (2022) 3577. http://doi:10.3390/en15103577.

[21] D. Garcia, D. Liang, C.R. Vistas, H. Costa, M. Catela, B.D. Tibúrcio, J. Almeida, Ce:Nd:YAG solar laser with 4.5% solar-to-laser conversion efficiency, Energies 15 (14) (2022) 5292, https://doi.org/10.3390/en15145292.

[22] Z. Cai, C. Zhao, Z. Zhao, J. Zhang, Z. Zhang, H. Zhang, Efficient 38.8 W/m^2 solar pumped laser with a Ce:Nd:YAG crystal and a Fresnel lens, Opt Express 31 (2) (2023) 1340–1353. http://doi:10.1364/OE.481590.

[23] P. Samuel, T. Yanagitani, H. Yagi, H. Nakao, Ken Ichi Ueda, S.M. Babu, Efficient energy transfer between Ce^{3+} and Nd^{3+} in cerium codoped Nd: YAG laser quality transparent ceramics, J. Alloys Compd. 507 (2) (2010) 475–478, https://doi.org/10.1016/j.jallcom.2010.07.207.

[24] T. Masuda, M. Iyoda, Y. Yasumatsu, S. Dottermusch, I.A. Howard, B.S. Richards, J. F. Bisson, M. Endo, A fully planar solar pumped laser based on a luminescent solar collector, Commun. Phys. 3 (2020) 60, https://doi.org/10.1038/s42005-020-0326-2.

[25] D. Garcia, D. Liang, J. Almeida, M. Catela, H. Costa, B.D. Tibúrcio, E. Guillot, C. R. Vistas, Lowest-threshold solar laser operation under cloudy sky condition, Renew. Energy 210 (2023) 127–133, https://doi.org/10.1016/j.renene.2023.03.124.

[26] ASTM G173-03, Standard Tables for Reference Solar Spectral Irradiances: Direct Normal and Hemispherical on 37◦ Tilted Surface, ASTM International, West Conshohocken, Pennsylvania, 2012. ASTM G173-03, https://www.astm.org/g0173-03r20.html.

[27] Y. Tai, G. Zheng, H. Wang, J. Bai, Near-infrared quantum cutting of Ce^{3+}– Nd^{3+} co-doped $Y_3Al_5O_{12}$ crystal for crystalline silicon solar cells, J. Photochem. Photobiol., A 303–304 (2015) 80–85, https://doi.org/10.1016/j.jphotochem.2015.02.009.

[28] M. Weksler, J. Shwartz, Solar-pumped solid-state lasers, IEEE J. Quantum Electron. 24 (6) (1988) 1222–1228, https://doi.org/10.1109/3.247.

[29] S. Payziyev, A. Sherniyozov, Influence of thermal population of lower laser levels on the performance of end-side-pumped Ce:Nd:YAG solar laser, J. Photonics Energy. 12 (4) (2022) 044501. http://doi:10.1117/1.Jpe.12.044501.

[30] Y. Song, J. Du, R. Yang, C. Lin, W. Chen, Z. Wu, H. Lin, X. Chen, Y. Zhuang, R.-J. Xie, Recyclable time–temperature indicator enabled by light storage in particles, Adv. Optical Mater. 11 (2023) 2202654, https://doi.org/10.1002/adom.202202654.

[31] C. Wang, Y. Chen, Z. Jiang, et al., Experimental investigation of light storage of diffraction-free and quasi-diffraction-free beams in hot atomic gas cell, Front. Phys. 17 (2022) 22503, https://doi.org/10.1007/s11467-021-1113-6.

[32] N. Pirrone, F. Bella, S. Hernández, Solar H_2 production systems: current status and prospective applications, Green Chem. 24 (2022) 5379. —5402, https://pubs.rsc.org/en/content/articlelanding/2022/gc/d2gc00292b.